



# Giant conductivity anisotropy in cubic $\text{CuCr}_2\text{Te}_3\text{I}$ and semiconducting behavior in $\text{CuCr}_2\text{S}_3\text{Cl}$ and $\text{CuCr}_2\text{Se}_3\text{Br}$

David J. Singh <sup>\*</sup>*Albuquerque, New Mexico 87110, USA* (Received 3 October 2023; revised 25 November 2023; accepted 8 December 2023; published 20 December 2023)

Spinel structure  $\text{CuCr}_2\text{X}_4$  where  $X$  is a chalcogen are ferromagnetic metals with Curie temperatures at or above room temperature. Experiments show that these compounds can be alloyed with halogens while preserving the ferromagnetic ordering. This alloying changes the carrier concentration and yields semiconductors for 25% halogen substitution on the chalcogen site in at least some cases. Here, we establish the electronic structures and related properties of  $\text{CuCr}_2\text{S}_3\text{Cl}$ ,  $\text{CuCr}_2\text{Se}_3\text{Br}$ , and  $\text{CuCr}_2\text{Te}_3\text{I}$ .  $\text{CuCr}_2\text{S}_3\text{Cl}$  and  $\text{CuCr}_2\text{Se}_3\text{Br}$  are ferromagnetic semiconductors with moderate band gaps and spin-polarized band edges. In contrast,  $\text{CuCr}_2\text{Te}_3\text{I}$  is found to be a semimetal, with nearly compensating Fermi surfaces. Calculations with spin-orbit coupling show an extraordinary sensitivity of the Fermi surfaces to the magnetization direction in this cubic material due to the details of the band crossings near the zone center. As a result,  $\text{CuCr}_2\text{Te}_3\text{I}$  is expected to show unusual anisotropic transport.

DOI: [10.1103/PhysRevB.108.214422](https://doi.org/10.1103/PhysRevB.108.214422)

## I. INTRODUCTION

There is ongoing interest in ferromagnetic semiconductors for spintronic applications [1]. There is also strong interest in such materials and in ferromagnetic semimetals for fundamental magnetotransport studies. Spinel structure  $\text{CuCr}_2\text{Se}_4$  doped with Br has attracted attention in this regard [2–4]. The chalcospinel compounds  $\text{CuCr}_2\text{S}_4$ ,  $\text{CuCr}_2\text{Se}_4$ , and  $\text{CuCr}_2\text{Te}_4$  are known ferromagnetic metals with cubic structures [4–12].  $\text{CuCr}_2\text{Te}_4$  has recently attracted attention due to the observation of metallic ferromagnetism at room temperature in thin sheets [11].

The chalcogen sites in these compounds can be alloyed with halogens while maintaining the ferromagnetism, at least in the case of alloying with the halogen in the same row of the periodic table as the chalcogen [2,3,13–19]. These are believed to be random alloys, without evidence for chalcogen-halogen ordering. Among the alloys with 3:1 chalcogen:halogen stoichiometry,  $\text{CuCr}_2\text{Se}_3\text{Br}$  has been experimentally characterized in the most detail. Importantly, it is ferromagnetic. This composition has been demonstrated to be insulating both in terms of transport and optical properties [13,14,20]. However, it should be noted that while experiments suggest semiconducting behavior, this is complicated by disorder, and in particular Lee and co-workers noted that they do not obtain activated behavior in samples close to the nominal semiconducting stoichiometry [2]. The halogen alloys of  $\text{CuCr}_2\text{S}_4$  and  $\text{CuCr}_2\text{Te}_4$  are thought to behave qualitatively similarly, although they have been less studied. Here, we investigate the 3:1 alloys using first-principles methods. We find that  $\text{CuCr}_2\text{S}_3\text{Cl}$  and  $\text{CuCr}_2\text{Se}_3\text{Br}$  are semiconducting ferromagnets with spin-polarized band edges, and

different spin polarizations for the conduction and valence band edges.  $\text{CuCr}_2\text{Te}_3\text{I}$  found to be a semimetal with nearly compensating spin-polarized Fermi surfaces that lead to an exceptionally large conductivity anisotropy due to spin-orbit coupling (SOC).

## II. COMPUTATIONAL METHODS

The present calculations were performed within density functional theory (DFT) using the general potential linearized augmented plane-wave (LAPW) method [21], as implemented in the WIEN2K code [22]. The generalized gradient approximation of Perdew, Burke, and Ernzerhof (PBE-GGA) [23] was employed. We did not apply a Hubbard  $U$  because the base materials are metallic chalcogenides, as opposed to antiferromagnetic insulating oxides, and in such cases, particularly for transition metals in the early part of the  $3d$  series (such as Cr and Fe), Hubbard  $U$  corrections can give spurious results including exaggerated magnetic properties [24,25]. Local orbitals were used to treat semicore states. This was based on the standard LAPW+lo augmentation [26], rather than the more efficient, but sometimes less accurate, APW+lo approach [27]. We used a plane-wave sector basis set cutoff  $k_{\text{max}}$  as given by the parameter  $R_{\text{min}}k_{\text{max}} = 9$ , where  $R_{\text{min}}$  is the smallest of the LAPW sphere radii. The reported results were obtained at the experimental lattice parameters for the cubic spinel structure [13]. The Cu and Cr atoms are on symmetry sites in these compounds with space group  $Fd\bar{3}m$  (227). The mixed chalcogen-halogen is at site  $32e$  ( $u, u, u$ ) with a free internal coordinate  $u$ . The internal coordinates were relaxed by total energy minimization. Reference calculations for the nonalloyed compounds  $\text{CuCr}_2\text{S}_4$ ,  $\text{CuCr}_2\text{Se}_4$ , and  $\text{CuCr}_2\text{Te}_4$  were performed by the same method, again using experimental lattice parameters [28] and relaxed internal parameters. The structural parameters are given in Table I.

<sup>\*</sup>david.joseph.singh@gmail.com

TABLE I. Basic properties of the chalco- and chalcogenide spinels, as obtained in scalar relativistic calculations. Results for the tellurides with SOC are given in the text. The lattice parameters are from experiment, while the internal parameter for the anion position,  $u$ , is from relaxation. Here, Cu (8b) is at (3/8, 3/8, 3/8), C (16c) is at (0,0,0), and the anion  $X$  (32e) is at ( $u, u, u$ ). A gap,  $E_g$ , of 0 denotes a metal. Spin magnetizations  $M$  are in  $\mu_B$  per formula unit, and the densities of states at the Fermi level,  $N_\uparrow(E_F)$  and  $N_\downarrow(E_F)$ , are in  $\text{eV}^{-1}$  per formula unit.

Compound	$a$ (Å)	$u$	$M$	$E_g$ (eV)	$N_\uparrow(E_F)$	$N_\downarrow(E_F)$
CuCr <sub>2</sub> S <sub>4</sub>	9.812	0.2421	5.02	0	1.78	0.25
CuCr <sub>2</sub> Se <sub>4</sub>	10.335	0.2425	5.11	0	2.07	0.39
CuCr <sub>2</sub> Te <sub>4</sub>	11.125	0.2429	5.31	0	2.37	0.60
CuCr <sub>2</sub> S <sub>3</sub> Cl	9.866	0.2418	6.00	0.40	0	0
CuCr <sub>2</sub> Se <sub>3</sub> Br	10.414	0.2420	6.00	0.37	0	0
CuCr <sub>2</sub> Te <sub>3</sub> I	11.120	0.2428	5.99	0	0.31	0.10

The alloying was treated by the virtual crystal approximation (VCA) [29–31]. The VCA is an average potential approximation. In the present case, it was applied by replacing the mixed chalcogen-halogen site by a site with an average nuclear charge  $Z_{vc} = Z_{Ch} + 0.25$ , where  $Z_{Ch}$  is the chalcogen atomic number. Thus,  $Z_{vc} = 16.25$  for CuCr<sub>2</sub>S<sub>3</sub>Cl,  $Z_{vc} = 34.25$  for CuCr<sub>2</sub>Se<sub>3</sub>Br, and  $Z_{vc} = 52.25$  for CuCr<sub>2</sub>Te<sub>3</sub>I.

The VCA goes beyond rigid bands, and specifically includes composition-dependent distortions of the band structure. In all electron implementations, the VCA is applicable to adjacent elements in the periodic table. It works best when the bands associated with the alloyed elements, in this case the chalcogen and halogen  $p$  bands, are broad and the elements are similar in electronic structure and chemical properties such as atomic size. It is helpful for the accuracy of the VCA if the two elements in question are similar in size. This is the case for adjacent chalcogen and halogen ions, specifically Shannon ionic crystal radii of 1.70, 1.84, and 2.07 Å, for S<sup>2-</sup>, Se<sup>2-</sup>, and Te<sup>2-</sup>, respectively, as compared to 1.67, 1.82, and 2.06 Å, for the corresponding halide ions, Cl<sup>-</sup>, Br<sup>-</sup>, and I<sup>-</sup>, respectively [32]. This is also supported in the present compounds by the fact that the experimental lattice parameters of the reference and corresponding halogen alloyed compounds are very similar (see Table I). The VCA has the advantage of maintaining the full crystal symmetry, which facilitates analysis of the band structure and Fermiology. This is essential for the characterization of the semimetallic state that we find for CuCr<sub>2</sub>Te<sub>3</sub>I in particular.

### III. RESULTS AND DISCUSSION

The scalar relativistic band structures are shown in Fig. 1. The values of the calculated spin magnetization, per formula unit, and the majority and minority densities of states at the Fermi level are given in Table I. These values were obtained using a  $32 \times 32 \times 32$  uniform grid for sampling the Brillouin zone. The band structures for the reference nonalloyed compounds are similar to those given in prior first-principles work [33–38]. As discussed previously for CuCr<sub>2</sub>Se<sub>4</sub>, the electronic structure from DFT calculations, similar to those reported here, is consistent with spectroscopic

measurements [39]. The spin magnetizations for these reference compounds are close to, but somewhat larger than, the nominal value for high-spin Cr<sup>+3.5</sup> ( $2.5\mu_B/\text{Cr}$ ), which would correspond to a model  $\text{Cu}^+\text{Cr}_2^{+3.5}\text{Ch}_4^{-2}$ . This picture is consistent with the Cr-derived metallic bands at the Fermi level. The values, slightly larger than  $2.5\mu_B/\text{Cr}$ , are also consistent with recent experiments [2] for CuCr<sub>2</sub>Se<sub>4</sub>. However, it should be noted that there is also significant covalency evident in the density of states, particularly between the chalcogens and both Cu and Cr. This leads to a moment larger than  $2.5\mu_B$  when integrated around the Cr atom, for example, in CuCr<sub>2</sub>Se<sub>4</sub>,  $2.72\mu_B$  inside a Cr LAPW sphere of radius 2.25 bohrs, enhanced slightly by an interstitial magnetization, and reduced by opposite polarizations of  $-0.15\mu_B$  for each Se (radius 2.25 bohrs) and  $-0.12\mu_B$  for each Cu (radius 2.20 bohrs). The magnetization increases with halogen alloying, reaching  $6\mu_B/\text{f.u.}$  for CuCr<sub>2</sub>S<sub>3</sub>Cl and CuCr<sub>2</sub>Se<sub>3</sub>Br, and  $5.99\mu_B$  for CuCr<sub>2</sub>Te<sub>3</sub>I. These values are consistent with recent experimental measurements [2] for CuCr<sub>2</sub>Se<sub>3</sub>Br.

As mentioned, the band structures for the nonalloyed reference compounds are metallic and have significant spin polarization with much lower values of the minority spin density of states at the Fermi level,  $N_\downarrow(E_F)$ , than for the majority spin,  $N_\uparrow(E_F)$ . The density of states spin polarization for CuCr<sub>2</sub>Se<sub>4</sub> is  $P_{\text{DOS}} = [N_\uparrow(E_F) - N_\downarrow(E_F)]/[N_\uparrow(E_F) + N_\downarrow(E_F)] = 0.61$ . This is consistent with the values  $|P| > 0.56$  found in point contact Andreev reflection measurements [4].

The band structures of the halogen alloyed compounds are shown in the middle row of Fig. 1. The corresponding projected electronic densities of states are given in the bottom row. We find that CuCr<sub>2</sub>S<sub>3</sub>Cl and CuCr<sub>2</sub>Se<sub>3</sub>Br are semiconductors. However, surprisingly, CuCr<sub>2</sub>Te<sub>3</sub>I has no gap and is a low carrier density semimetal. The band structures of the halogenated compounds cannot be understood based on rigid band electron doping of the reference compounds. For example, the band structure of CrCr<sub>2</sub>Se<sub>4</sub> shows a substantial gap in the majority spin channel above the Fermi level, while the minority spin bands do not show a full gap. This feature has led to the expectation that the material would become a half-metal upon electron doping, for example, with halogen alloying [39]. Half-metallicity was also suggested with Se vacancies [37]. This suggested a potential for spintronic applications.

Instead, we find that the rigid band picture does not apply. First of all, as might be expected, the exchange splitting between the majority and minority spin bands increases modestly as the Cr moments increase (see Table I) with electron count. This can be seen in Fig. 1, where the majority bands occur lower relative to the conduction band edges than would be expected from the reference compound band structure. Second, there is a strong distortion of the bands, which opens a gap in the minority spin near the Fermi level, converting what would be a half-metal into a semiconductor. This means that the expected large range of half-metallicity from the rigid band model is not found. This is consistent with point contact Andreev measurements for CuCr<sub>2</sub>Se<sub>3</sub>Br where high-spin polarization but not as high as expected for a half-metal was found [4].

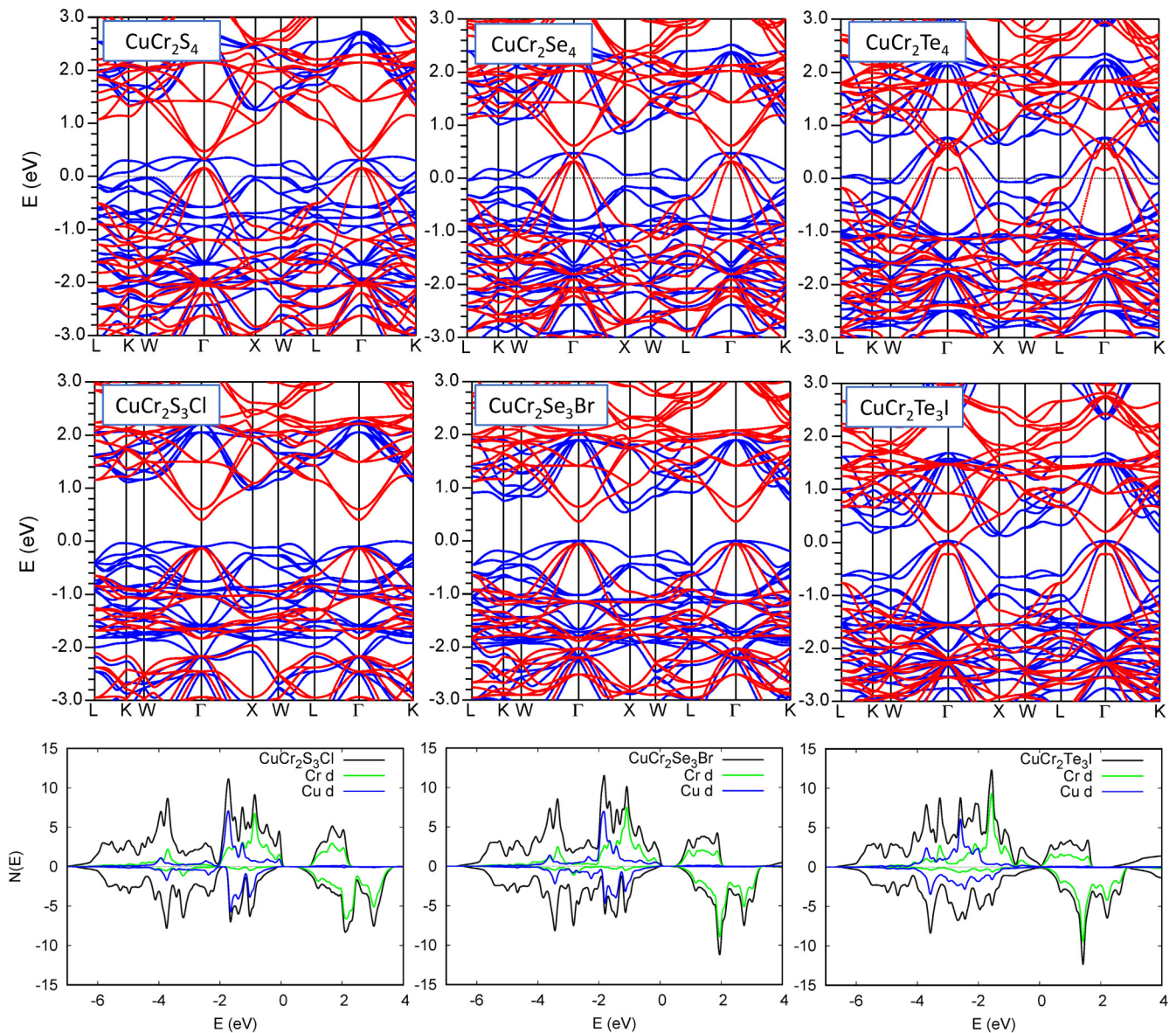


FIG. 1. Scalar relativistic band structures. Majority spin bands are shown in blue while minority spin bands are red. The zero energy is the Fermi level for metals, and the valence band maximum for semiconductors. Note the semimetallic character of  $\text{CuCr}_2\text{Te}_3\text{I}$ . The corresponding projected densities of states are given in the bottom row for the chalcogenides. Majority spin is shown as positive and minority spin is shown as negative.

The projected densities of states (bottom row of Fig. 1) show Cu  $d$  bands between approximately  $-2$  and  $0$  eV, with respect to the valence band edge in  $\text{CuCr}_2\text{S}_3\text{Cl}$  and  $\text{CuCr}_2\text{Se}_3\text{Br}$ .  $\text{CuCr}_2\text{Te}_3\text{I}$  shows a broader distribution of the Cu  $d$  states, extending from approximately  $-4$  to  $-1$  eV with respect to the Fermi level  $E_F$ . In all three of these compounds, the Cr  $d$  distribution is consistent with high-spin  $\text{Cr}^{+3}$  with an occupied majority spin Cr  $t_{2g}$  level and unoccupied  $e_g$  and minority spin  $t_{2g}$  bands (note that there is a slight overlap in semimetallic  $\text{CuCr}_2\text{Te}_3\text{I}$ , as discussed below).

As mentioned,  $\text{CuCr}_2\text{S}_3\text{Cl}$  and  $\text{CuCr}_2\text{Se}_3\text{Br}$  show semiconducting gaps in our VCA calculations. Figure 1 shows that the band edges are spin polarized in these compounds, with the valence band edges coming from majority spin bands, while the conduction band edges come from minority spin

bands. While this might suggest some device applications based on  $p$ - $n$  junctions, we note that the semiconducting composition corresponds to very heavy 25% alloying between elements with different valence states. As such, strong carrier scattering might be expected. This would make it difficult to realize devices requiring good carrier transport. Experimental resistivity measurements show high resistivity in a range of composition near the semiconducting stoichiometry with evidence for disorder-induced carrier localization [2]. One possible remaining application direction would be to use the high-spin polarization that would be expected very close to the semiconducting composition. In principle, it may be possible to use  $p$ -type material as a source of majority spin carriers in a device and  $n$ -type material as a source of minority spin carriers. Perhaps in this context the availability of a single

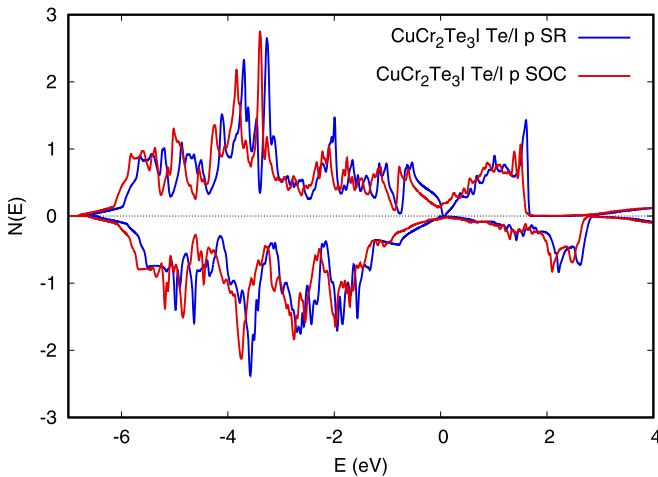


FIG. 2. Anion (Te/I)  $p$  component of the density of states for ferromagnetic VCA  $\text{CuCr}_2\text{Te}_3\text{I}$  comparing the scalar relativistic (SR) result with that including SOC. Note that this is obtained by projection onto  $p$  character within Te/I centered LAPW spheres of radius 2.40 bohrs. The plot is on a per formula unit, per spin basis with the Fermi level set to 0 eV.

material that with slightly different compositions can provide both majority and minority spin carriers could enable some applications.

We now turn to  $\text{CuCr}_2\text{Te}_3\text{I}$ , which is semimetallic in our scalar relativistic VCA calculation. The semimetallic nature arises from a minority spin band that intersects the majority spin band that would correspond to the valence band maximum around the  $\Gamma$  point. In addition there is a near touching of the Fermi energy by an unoccupied minority spin band at the  $X$  point. The band crossing near the  $\Gamma$  point leads to three hole Fermi surfaces of majority spin character and one compensating minority spin Fermi surface. The occupancies of the hole sections (per two formula unit unit cell) are 0.0002, 0.0063, and 0.0070 holes, while the minority spin section contains 0.0136 electrons.

The fact that  $\text{CuCr}_2\text{Te}_3\text{I}$  is a low carrier density ferromagnetic semimetal and includes the relatively high atomic number  $p$  electron elements, Te and I, suggests that spin-orbit coupling (SOC) may be important for its properties. Besides modification of the bands, SOC mixes majority and minority spin bands, and in a ferromagnet this mixing depends on the magnetization direction. Accordingly, we did calculations including SOC to investigate this. We find that the magnetic properties are only slightly changed by SOC, and that the band structure remains semimetallic.

The role of the Te/I atoms for the SOC is supported by the electronic density of states. Figure 2 shows the  $p$  projection for the anion LAPW spheres, comparing scalar relativistic calculations and calculations with SOC (magnetization along the [001] direction). It should be noted that this projection, while proportional to the Te/I  $p$  orbital character is an underestimate as anion  $p$  states are extended and as a result some of the Te/I  $p$  character will be outside the projection radius. In any case, it may be seen that there is evidence of significant hybridization involving the anions, for example, in the Te/I contribution to the electronic structure above the Fermi level.

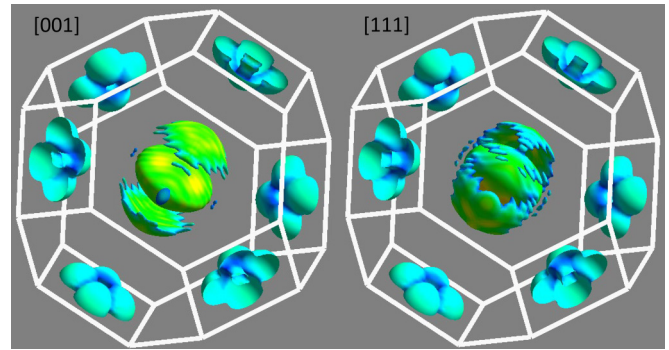


FIG. 3. Fermi surfaces for  $\text{CuCr}_2\text{Te}_3\text{I}$  calculated with SOC and magnetization directions along [001] (left) and [111] (right). The surfaces are shaded by velocity from blue (low) to red (high). This figure was generated by the FERMISURFER software [40].

It is also seen in the fact that there is noticeable exchange splitting of the Te/I density of states, particularly above the Fermi level and in fact that the majority and minority spin contributions in the occupied electronic states within approximately 2 eV of the Fermi level are significantly different. It may also be noted that the Te/I contribution at the Fermi level especially for the majority spin is significantly affected by SOC. Furthermore, the induced magnetic moments in the Te/I spheres while not large (approximately  $-0.08\mu_B$ /sphere, where the negative sign denotes the fact that they are opposite to the overall spin magnetization direction), are nonetheless significant. We additionally find small orbital moments on the Te/I of approximately  $-0.0004\mu_B$ /sphere.

The calculated spin moment (including SOC with magnetization direction along [001]) becomes  $5.98\mu_B$  per formula unit. The Cr orbital moments are very small,  $0.03\mu_B/\text{Cr}$ , consistent with a nearly half full  $t_{2g}$  shell, and parallel to the spin moments. However, in spite of the small orbital moments, there is a significant magnetization direction-dependent effect on the Fermi surface as shown in Fig. 3. The inclusion of SOC leads to interaction between the majority spin Fermi surfaces and the minority spin surface that results in gapping in the directions away from the magnetization direction. The inner large sheet Fermi surface then becomes flattened along the magnetization direction, while the other two sheets that originated from the largest majority section without SOC, and the minority section break up leaving a shell-like relatively high velocity surface along the magnetization direction. This structure rotates with the magnetization direction as seen comparing the left and right panels of Fig. 3. An additional effect of SOC is the appearance of small low Fermi velocity sections around the  $X$  points. There are four bands crossing the Fermi level, similar to the scalar relativistic result, but the band occupancies are somewhat changed. For magnetization along [001] the band occupancies are 0.9975 (corresponding to 0.0025 holes), 0.9957 (0.0043 holes), 0.9811 (0.0189 holes), and 0.0257 electrons.

The Fermi surface structure with SOC thus takes a visibly anisotropic structure. This anisotropy may then be expected to yield a conductivity anisotropy, with conductivity higher along the magnetization direction considering the fact that the Fermi surface has more area normal to the magnetization. The

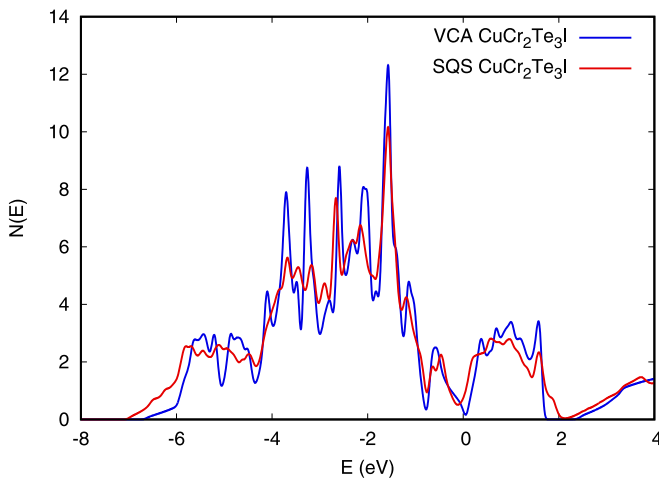


FIG. 4. Comparison of the total density of states of ferromagnetic  $\text{CuCr}_2\text{Te}_3\text{I}$  as obtained from calculations in the VCA and with an SQS cell, including SOC. The plot is on a per formula unit, per spin basis with the Fermi level set to 0 eV.

magnetic anisotropy is low in cubic materials, such as these spinels. As such, the magnetization can be readily rotated by magnetic fields, which then might be expected to lead to exceptional magnetotransport effects below the Curie temperature in this material if the conductivity anisotropy is sizable. We calculated the conductivity anisotropy within the constant scattering time approximation (CSTA) using the BOLTZTRAP code [41]. The CSTA assumes that the relaxation time is the same for all states on the Fermi surface, so that the anisotropy comes from integration of the band velocities on the Fermi surface. For this calculation we used the first-principles electronic structure on a dense  $32 \times 32 \times 32$  grid of  $\mathbf{k}$  points. We find giant anisotropy of the conductivity for a cubic material. For a [001]-oriented magnetization the anisotropy is  $\sigma_z/\sigma_{x,y} = 1.56$  (here,  $z$  is the magnetization direction).

In addition to the VCA calculations discussed above, we did calculations for a special quasirandom structure (SQS) in order to verify that local symmetry breaking due to com-

positional disorder would not destroy the semimetallic state predicted by the VCA calculations. Such local symmetry breaking has been discussed recently in the context of metal-insulator transitions [42]. For this purpose, we generated a 14-atom SQS structure for  $\text{CuCr}_2\text{Te}_3\text{I}$  using the Monte Carlo method implemented in the ATAT code [43,44]. The atomic coordinates were relaxed and electronic structure calculations performed including SOC with the magnetization direction along [001]. The low symmetry of the SQS cell leads to non-negligible relaxations, so that for example the shortest Cr-Te bond is 2.66 Å, while the shortest Cr-I bond is 2.78 Å. Nonetheless, we find that the semimetallic character is retained as shown in the density of states (Fig. 4), where distortion and broadening of the peaks related to disorder is evident, but the semimetallic nature is preserved. The spin magnetization of the SQS cell is  $5.996\mu_B$  per formula unit, which is slightly larger than the  $5.983\mu_B$  obtained in the VCA calculation.

#### IV. SUMMARY AND CONCLUSIONS

We report DFT calculations using the VCA for halogen alloyed spinels,  $\text{CuCr}_2\text{S}_3\text{Cl}$ ,  $\text{CuCr}_2\text{Se}_3\text{Br}$ , and  $\text{CuCr}_2\text{Te}_3\text{I}$ . We find semiconducting states with small band gaps of  $\sim 0.4$  eV for the S and Se compounds, along with oppositely spin-polarized conduction and valence band edges.  $\text{CuCr}_2\text{Te}_3\text{I}$  is found to be a low carrier density semimetal. The particular band structure of this compound leads to a Fermi surface that strongly reconstructs due to SOC. This is predicted to lead to an exceptionally large conductivity anisotropy for a cubic material. It will be of interest to measure this in magnetized samples, and if demonstrated to explore magnetotransport effects, for example, with fields transverse to the magnetization direction. Considering the possibly strong scattering from chalcogen-halogen disorder, it would also be of interest to investigate alternate methods of electron doping  $\text{CuCr}_2\text{Te}_4$ , in particular methods that do not involve halogen substitution for Te. One approach might be substitution on the Cu site. To our knowledge,  $\text{ZnCr}_2\text{Te}_4$  is not a reported spinel compound, though the present results suggest that it may be of interest to attempt its synthesis and if successful explore its properties.

- [1] A. Hirohata, K. Yamada, Y. Nakatani, I.-L. Prejbeanu, B. Diény, P. Pirro, and B. Hillebrands, *J. Magn. Magn. Mater.* **509**, 166711 (2020).
- [2] W.-L. Lee, S. Watauchi, V. L. Miller, R. J. Cava, and N. P. Ong, *Science* **303**, 1647 (2004).
- [3] W.-L. Lee, S. Watauchi, V. L. Miller, R. J. Cava, and N. P. Ong, *Phys. Rev. Lett.* **93**, 226601 (2004).
- [4] K. Borisov, J. Alaria, J. M. D. Coey, and P. Stamenov, *J. Appl. Phys.* **115**, 17C717 (2014).
- [5] F. K. Lotgering, in *Proceedings of the International Conference on Magnetism, Nottingham, UK, 1964* (Physical Society of London, London, 1964), p. 553.
- [6] M. Robbins, H. W. Lehmann, and J. G. White, *J. Phys. Chem. Solids* **28**, 897 (1967).
- [7] F. Lotgering and R. van Staple, *Solid State Commun.* **5**, 143 (1967).
- [8] I. Nakatani, H. Nosé, and K. Masumoto, *J. Phys. Chem. Solids* **39**, 743 (1978).
- [9] T. Suzuyama, J. Awaka, H. Yamamoto, S. Ebisu, M. Ito, T. Suzuki, T. Nakama, K. Yagasaki, and S. Nagata, *J. Solid State Chem.* **179**, 140 (2006).
- [10] Y. Zhang, Y. Hu, Z. Deng, Z. Lou, Y. Hou, and F. Teng, *Mater. Lett.* **310**, 131478 (2022).
- [11] H. Wang, Y. Wen, X. Zhao, R. Cheng, L. Yin, B. Zhai, J. Jiang, Z. Li, C. Liu, F. Wu, and J. He, *Adv. Mater.* **35**, 2211388 (2023).
- [12] M. Esters, A. Liebig, J. J. Ditto, M. Falmbigl, M. Albrecht, and D. C. Johnson, *J. Alloys Compd.* **671**, 220 (2016).
- [13] K. Miyatani, K. Minematsu, Y. Wada, F. Okamoto, K. Kato, and P. K. Baltzer, *J. Phys. Chem. Solids* **32**, 1429 (1971).
- [14] K. Miyatani, Y. Wada, and F. Okamoto, *J. Phys. Soc. Jpn.* **25**, 369 (1968).
- [15] J. G. White and M. Robbins, *J. Appl. Phys.* **39**, 664 (1968).

- [16] M. Robbins, P. K. Baltzer, and E. Lopatin, *J. Appl. Phys.* **39**, 662 (1968).
- [17] J. Granot, *Phys. Lett. A* **43**, 269 (1973).
- [18] H. Brändle, J. Schoenes, P. Wachter, F. Hulliger, and W. Reim, *J. Magn. Magn. Mater.* **93**, 207 (1991).
- [19] H. Han, L. Zhang, W. Tong, Z. Qu, C. Zhang, L. Pi, and Y. Zhang, *J. Alloys Compd.* **685**, 304 (2016).
- [20] T. H. Lee, R. M. Gluck, R. K. Ahrenkiel, and T. J. Coburn, *AIP Conf. Proc.* **5**, 274 (1972).
- [21] D. J. Singh and L. Nordstrom, *Planewaves, Pseudopotentials and the LAPW Method*, 2nd ed. (Springer, Berlin, 2006).
- [22] P. Blaha, K. Schwarz, F. Tran, R. Laskowski, G. K. H. Madsen, and L. D. Marks, *J. Chem. Phys.* **152**, 074101 (2020).
- [23] J. P. Perdew, K. Burke, and M. Ernzerhof, *Phys. Rev. Lett.* **77**, 3865 (1996).
- [24] M. Cococcioni and S. de Gironcoli, *Phys. Rev. B* **71**, 035105 (2005).
- [25] Y. Fu and D. J. Singh, *Phys. Rev. B* **100**, 045126 (2019).
- [26] D. Singh, *Phys. Rev. B* **43**, 6388 (1991).
- [27] E. Sjöstedt, L. Nordstrom, and D. J. Singh, *Solid State Commun.* **114**, 15 (2000).
- [28] T. Kanomata and H. Ido, *J. Phys. Soc. Jpn.* **36**, 1322 (1974).
- [29] J. A. Van Vechten and T. K. Bergstresser, *Phys. Rev. B* **1**, 3351 (1970).
- [30] B. Winkler, C. Pickard, and V. Milman, *Chem. Phys. Lett.* **362**, 266 (2002).
- [31] J. Kübler, *J. Magn. Magn. Mater.* **15-18**, 859 (1980).
- [32] R. D. Shannon, *Acta Crystallogr.* **A32**, 751 (1976).
- [33] J. I. Horikawa, T. Hamajima, F. Ogata, T. Kambara, and K. I. Gondaira, *J. Phys. C: Solid State Phys.* **15**, 2613 (1982).
- [34] F. Ogata, T. Hamajima, T. Kambara, and K. I. Gondaira, *J. Phys. C: Solid State Phys.* **15**, 3483 (1982).
- [35] V. N. Antonov, V. P. Antropov, B. N. Harmon, A. N. Yaresko, and A. Y. Perlov, *Phys. Rev. B* **59**, 14552 (1999).
- [36] T. Saha-Dasgupta, M. De Raychaudhury, and D. D. Sarma, *Phys. Rev. B* **76**, 054441 (2007).
- [37] J. Bettinger, R. Chopdekar, M. Liberati, J. Neulinger, M. Chshiev, Y. Takamura, L. Alldredge, E. Arenholz, Y. Idzerda, A. Stacy, W. Butler, and Y. Suzuki, *J. Magn. Magn. Mater.* **318**, 65 (2007).
- [38] Y. H. A. Wang, A. Gupta, M. Chshiev, and W. H. Butler, *Appl. Phys. Lett.* **92**, 062507 (2008).
- [39] S. Bordacs, I. Kezsmarki, K. Ohgushi, and Y. Tokura, *New J. Phys.* **12**, 053039 (2010).
- [40] M. Kawamura, *Comput. Phys. Commun.* **239**, 197 (2019).
- [41] G. K. H. Madsen and D. J. Singh, *Comput. Phys. Commun.* **175**, 67 (2006).
- [42] O. I. Malyi and A. Zunger, *Appl. Phys. Rev.* **7**, 041310 (2020).
- [43] A. van de Walle, M. D. Asta, and G. Ceder, *Calphad* **26**, 539 (2002).
- [44] A. van de Walle, P. Tiwary, M. M. de Jong, D. L. Olmsted, M. D. Asta, A. Dick, D. Shin, Y. Wang, L.-Q. Chen, and Z.-K. Liu, *Calphad* **42**, 13 (2013).